



Exceptional age constraint on a fossiliferous sedimentary succession preceding the Cretaceous Thermal Maximum

Ryan T. Tucker^{1,*}, James L. Crowley², Michael T. Mohr², Ray K. Renault¹, Peter J. Makovicky³, and Lindsay E. Zanno^{4,5}

¹Department of Earth Sciences, Stellenbosch University, Private Bag X1, Matieland, 7602, Stellenbosch, South Africa

²Department of Geosciences, 1910 University Drive, MS 1535, Boise State University, Boise, Idaho 83725, USA

³Department of Earth and Environmental Sciences, Suite 150, 116 Church Street SE, University of Minnesota, Minneapolis, Minnesota 55455, USA

⁴Paleontology, North Carolina Museum of Natural Sciences, 11 W. Jones Street, Raleigh, North Carolina 27601, USA

⁵Department of Biological Sciences, North Carolina State University, Campus Box 7617, Raleigh, North Carolina 27695, USA

ABSTRACT

Understanding the effects of climatic upheavals during the Early to Late Cretaceous transition is essential for characterizing the tempo of tectonically driven landscape modification and biological interchange; yet, current chronostratigraphic frameworks are too imprecise, even on regional scales, to address many outstanding questions. This includes the Mussentuchit Member of the uppermost Cedar Mountain Formation, central Utah (southwestern United States), which could provide crucial insights into these impacts within the Western Interior Basin of North America yet remains imprecisely constrained. Here, we present high-precision U-Pb zircon dates from four primary ash beds distributed across \sim 50 km in central Utah that better constrain the timing of deposition of the Mussentuchit Member and the age of entombed fossils. Ages for ash beds are interpreted through a combination of Bayesian depositional age estimation and stratigraphic age modeling, resulting in posterior ages from 99.490 ± 0.057 to 98.905 ± 0.158 Ma. The age model predicts probabilistic ages for fossil localities between the ashes, including new ages for *Moros intrepidus*, *Siats meekerorum*, and several undescribed ornithischian dinosaur species of key interest for understanding the timing of faunal turnover in western North America. This new geochronology for the Mussentuchit Member offers unprecedented temporal insights into a volatile interval in Earth's history.

INTRODUCTION

Climatic perturbations typically occur on the scale of tens to hundreds of thousands of years, much too short to be recorded in most stratigraphic records (Huybers, 2007, 2011; Hain et al., 2014). To address this, geoscientific studies have employed high-precision U-Pb zircon dating to resolve cryptic stratigraphic relationships and formulate meaningful temporal frameworks for climate reconstruction. Such initiatives are particularly interesting within the Western Interior Basin of North America, a mosaic of contemporaneous and highly fossiliferous sedimentary successions preserving multiple intervals of climate fluctuations (Miall, 2008; Schwartz et al., 2021; Singer et al., 2021).

The past several decades have seen intensifying efforts to constrain the world-famous vertebrate assemblages of the Campanian in the Western Interior Basin (e.g., Eberth and Kamo, 2020; Beveridge et al., 2022; Ramezani et al., 2022), resulting in marked improvements in our understanding of corresponding climatic and paleoenvironmental changes (predominantly cooling and aridification and their cascading effects on ecosystem evolution near the close of the Mesozoic; Wang et al., 2014; Barral et al., 2017). By comparison, refined correlations of terrestrial rocks spanning what is arguably the peak of Mesozoic global warming—the Cenomanian–Turonian Cretaceous Thermal Maximum (CTM)—have remained elusive.

One such sedimentary succession, the Mussentuchit Member of the uppermost Cedar Mountain Formation, central Utah (southwestern United States), might be an archive of the

Early–Late Cretaceous transitional climatic crisis (Fig. 1) (Laskowski et al., 2013; Kirkland et al., 2016; Tucker et al., 2020, 2022), but biostratigraphic calibration has remained tenuous, with local and transitional fauna mixed and as much as half of the local fauna representing range extensions (Cifelli et al., 1999). Radioisotopic dating of volcaniclastic sedimentary rocks has also met with mixed success, with the earliest efforts establishing ages of 98.39 ± 0.07 and 97.0 ± 0.1 Ma for the Mussentuchit Member from $^{40}\text{Ar}/^{39}\text{Ar}$ dating of plagioclase (Cifelli et al., 1997, 1999; recalibrated by Garrison et al., 2007). Recent attempts at temporal refinement using $^{206}\text{Pb}/^{238}\text{U}$ laser ablation–inductively coupled plasma–mass spectrometry (LA-ICP-MS) dating of detrital zircon from key fossil-bearing localities yielded relatively imprecise dates that are unrealistically too young, likely due to Pb loss (Tucker et al., 2020). Despite being essential for reconstructing patterns of biotic turnover and determining causal relationships with a host of potential forcers (including Western Interior Basin tectonism and shifting climate factors), uncertainty in the age of the Mussentuchit Member persists. Here we present a new temporal framework for the Mussentuchit Member using high-precision $^{206}\text{Pb}/^{238}\text{U}$ zircon dating of four stratigraphically significant ash beds (herein defined as Mussentuchit Ash Zones 1 through 4, MAZ1–MAZ4) and Bayesian age modeling.

GEOLOGY AND SAMPLING

The Mussentuchit Member is informally subdivided into a lower and upper unit, separated by the regionally extensive “middle sandstone” (Fig. 2) (Tucker et al., 2020, 2022). Four ash beds persist across \sim 50 km of the exposed regional outcrops (Figs. 1 and 2) despite

Ryan Thomas Tucker  <https://orcid.org/0000-0002-4232-1879>
*tucker@sun.ac.za

CITATION: Tucker, R.T., et al., 2023, Exceptional age constraint on a fossiliferous sedimentary succession preceding the Cretaceous Thermal Maximum: *Geology*, v. 51, p. 962–967, <https://doi.org/10.1130/G51278.1>

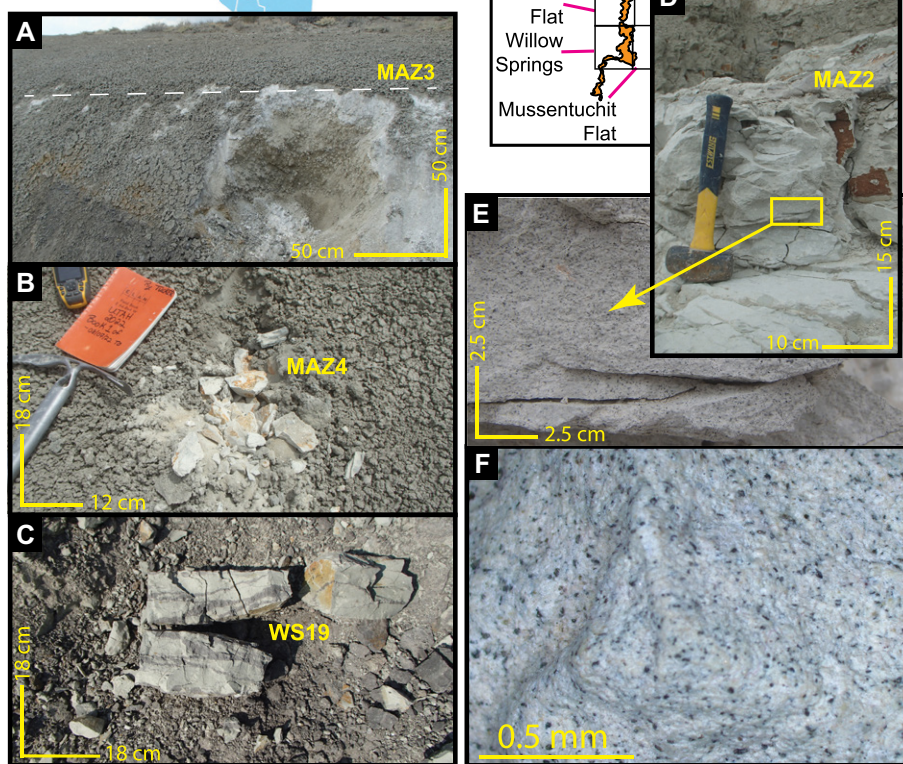
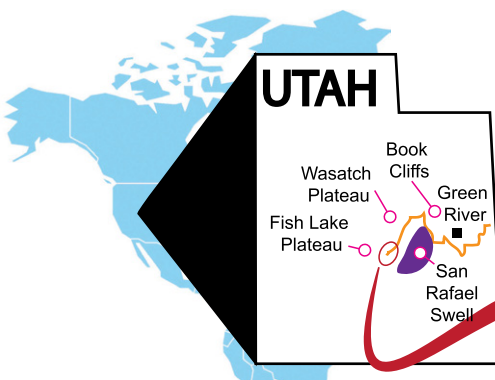


Figure 1. Study area in central Utah, southwestern United States. Exposures of Cedar Mountain Formation (CMF) are in orange (modified from Tucker et al., 2022). Labeled rectangles represent 7.5-minute quadrangles. (A) Exposure of Mussentuchit ash zone 3 (MAZ3). (B) Exposed bed of MAZ4 with surficial popcorn weathering. (C) Indurated and altered bentonite from sample site WS19. (D, E) 40-cm-thick MAZ2. (D) and closeup image (E) with visible phenocrysts. (F) Light microscope (2x magnification) photo of biotite, quartz, and feldspar phenocrysts along with visible glassy textures.

(1) regional tectonic deformation (synform-anti-form), (2) minor faulting, (3) downcutting by the overlying Naturita Formation, and (4) thinning of the Mussentuchit Member northward until it pinches out near Castle Dale, Utah. Three of the four laterally continuous altered ash layers were previously described for the Mussentuchit Wash 7.5-minute quadrangle (Garrison et al., 2007). Across the mapping area, the lowest ash bed (MAZ1) occurs 6–8 m above the basal contact and 1–2 m below the middle sandstone (uppermost lower Mussentuchit Member). The second ash bed (MAZ2) overlies the middle sandstone by 0.5–1.0 m. The third bed (MAZ3) is 5–7 m above the middle sandstone and 4–8 m below the contact with the overlying Naturita Formation.

The highest bed (MAZ4) is 0.5–1.0 m below the overlying contact with the Naturita Formation. Due to the variable erosional downcutting, MAZ4 is intermittently present (Garrison et al., 2007; Tucker et al., 2022). The ash beds range in thickness from 20 to 40 cm on average and weather to light green, drab gray, gray, dark gray, and light black. Haystack and surficial popcorn weathering are ubiquitous, along with internal jigsaw puzzle clay fractures and nodular masses. More detailed observations include: (1) visible waxy texture; (2) quartz, biotite, and plagioclase phenocrysts; (3) visible glass; (4) vesicles; (5) variation in internal layering; (6) clay charge; and (7) wet versus dry color modification (Fig. 1). Garrison et al. (2007) identified

three of the four as altered bentonites; however, based on our observations, all four are identified as tuffaceous K-bentonites (Huff, 2016; see the Supplemental Material¹, including Tables S1 (X-ray fluorescence [XRF] data) and S2 (X-ray diffraction [XRD] data) and Fig. S1). The 10 samples for U-Pb zircon geochronology were collected across ~50 km based on geographic distribution and stratigraphic position (GPS locations in Table S3). In addition to these four beds, we resampled historical sites WS19 (V826) and WS10 (V695), previously dated via $^{40}\text{Ar}/^{39}\text{Ar}$ and recalibrated by Garrison et al. (2007, p. 476).

U-Pb geochronology was conducted at the Isotope Geology Laboratory, Boise State University, Idaho, USA, using two U-Pb zircon analysis methods for most samples: LA-ICP-MS U-Pb dating of sharply faceted grains to identify the youngest grains, followed by chemical abrasion-isotope dilution-thermal ionization mass spectrometry (CA-ID-TIMS; Mattinson, 2005) to obtain precise U-Pb dates. Exceptions are sample COI-2, which yielded zircon too small for LA-ICP-MS and thus was dated by CA-ID-TIMS only, and sample WS19, which yielded only detrital zircon and thus was not dated. Details of the analytical methods and cathodoluminescence images of zircon grains are given in the Supplemental Material.

U-Pb GEOCHRONOLOGY

Zircon grains in the 10 samples from the four ash bed zones (MAZ1–MAZ4) vary in the proportion of sharply faceted grains, from nearly entirely sharply faceted grains that are likely primary pyroclastic zircon to nearly entirely round grains that are detrital zircon incorporated during post-depositional reworking (estimates are given in Table S4). Only six of the 281 sharply faceted grains dated by LA-ICP-MS were clearly detrital, demonstrating the effectiveness of this pre-screening approach for identifying the eruption-phase grains (Tables S5–S16). CA-ID-TIMS dates from 74 grains from 10 samples (Fig. 3; Table S4) are concordant and highly precise (average error on single analyses is ± 0.069 m.y. or 0.07%), primarily due to large amounts of radiogenic Pb (average in each grain is 18 pg) relative to common Pb (average is 0.15 pg). Most samples yielded a range of dates (spanning as much as 1.64 m.y.), with the young end of the spectra in each sample typically having two to six equivalent dates. Dispersion on the order of <200 k.y. can be attributed to a protracted magmatic residence and recycling of

¹Supplemental Material. All analytical results of all samples included within this study (LA-ICP-MS, CA-ID-TIMS, XRD, and XRF) along with CL zircon images with ablation spots indicated. Please visit <https://doi.org/10.1130/GEOL.S.23750286> to access the supplemental material, and contact editing@geosociety.org with any questions.

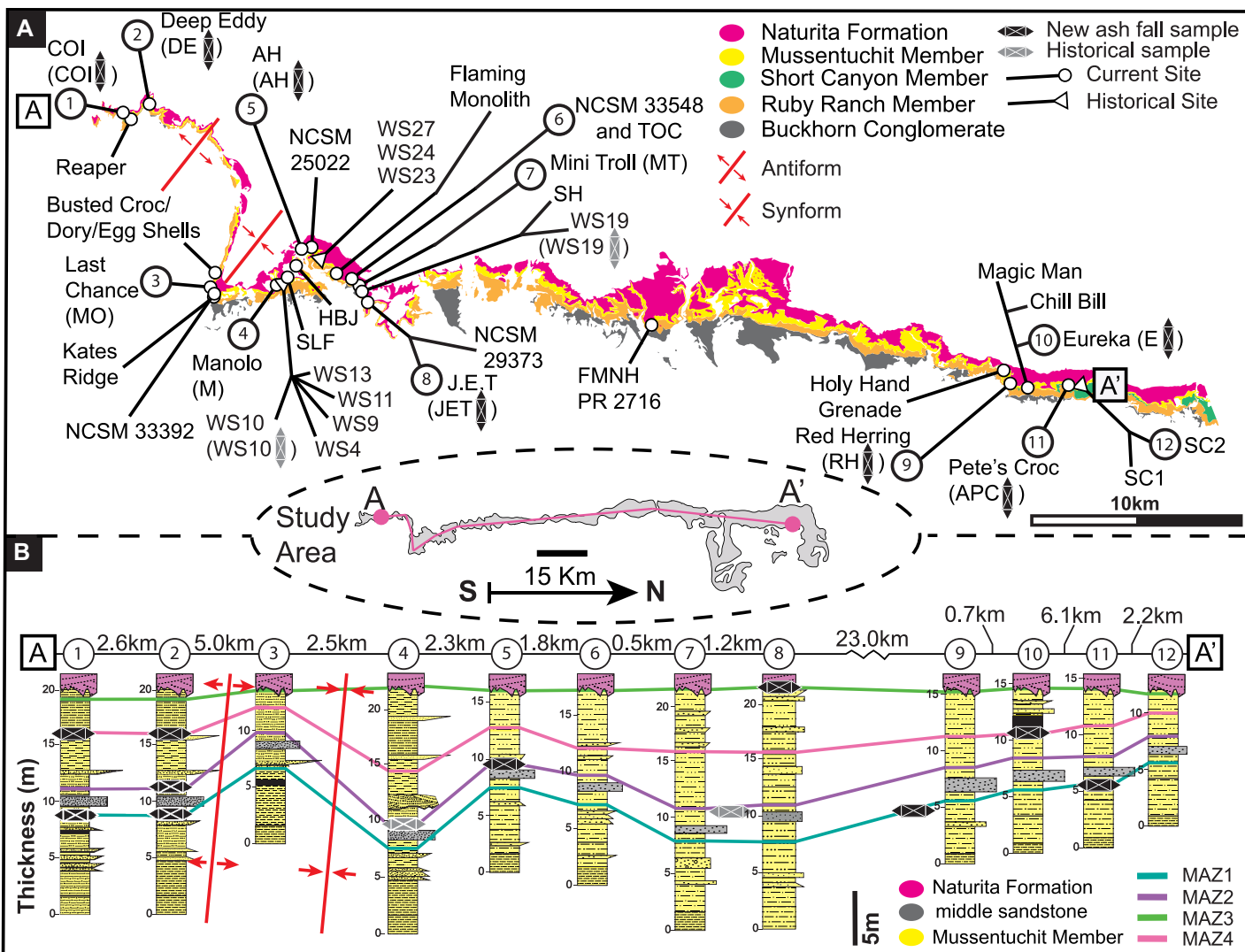


Figure 2. Geological map (A) and stratigraphic cross-section (A-A') (B) with correlations of each Mussentuchit ash zone (MAZ1-MAZ4) and locations of samples collected in 2021. Labels with zircon(s) and parentheses indicate samples analytically assessed via laser ablation-inductively coupled plasma-mass spectrometry and isotope chemical abrasion-dilution-thermal ionization mass spectrometry in this study. Geological map modified from Hintze et al. (2000) and Tucker et al. (2020, 2022).

zircon grains (e.g., Wotzlaw et al., 2014), while more significant amounts are likely due to the incorporation of epiclastic zircon during syn- or post-depositional reworking of the ash beds, evidenced by the considerable proportions of round, obviously detrital grains in some samples (Table S16) and the few LA-ICP-MS dates that indicate detrital origins.

Due to the difficulty in identifying the youngest statistical group of dates from complex distributions and lower- n data sets, we integrated all $^{206}\text{Pb}/^{238}\text{U}$ zircon dates within each ash zone with our composite stratigraphic column to construct an age model that generates stratigraphically conditioned posterior ages using Bayesian Markov Chain Monte Carlo statistics (e.g., Schoene et al., 2019, 2021). We first employed the Bayesian algorithm of Keller et al. (2018) to establish probabilistic eruption and depositional ages of 99.474 ± 0.052 Ma for MAZ1, 99.432 ± 0.079 Ma for MAZ2,

99.198 ± 0.053 Ma for MAZ3, and 98.881 ± 0.176 Ma for MAZ4 (2σ errors) (Fig. 3; Table S17), which were subsequently used as input likelihoods in the modified Bchron age model (Trayler et al., 2020; R Core Team, 2020). The outcomes of the age modeling are stratigraphically conditioned posterior ages of $99.490 \pm 0.057/-0.050$ Ma for MAZ1, $99.401 \pm 0.058/-0.066$ Ma for MAZ2, $99.191 \pm 0.057/-0.062$ Ma for MAZ3, and $98.905 \pm 0.158/-0.183$ Ma for MAZ4 (medians $\pm 95\%$ highest density intervals; Fig. 3B; Fig. 4; Table S18), which are our preferred ages for these ash beds.

IMPLICATIONS

Our probabilistic ages for the ash zones are consistent with superposition (Rossignol et al., 2019; Sharman and Malkowski, 2020; Vermeesch, 2021) and therefore interpreted as depositional ages. Age modeling results indicate

that accumulation of the Mussentuchit Member occurred between $99.674 \pm 0.439/-0.197$ and $98.905 \pm 0.158/-0.183$ Ma, for a duration of $776 \pm 421/-242$ k.y. Furthermore, the age model establishes probabilistic ages for fossil localities between the ash zones (Fig. 4). Most noteworthy are ages of $99.415 \pm 0.056/-0.059$ Ma for specimen NCSM 33392 (holotype of *Moros intrepidus*), $99.119 \pm 0.071/-0.139$ Ma for FMNH PR 2716 (holotype of *Siats meekerorum*), $99.652 \pm 0.413/-0.176$ Ma for NCSM 29373 (holotype of *Iani smithi*), $99.466 \pm 0.046/-0.053$ Ma for NCSM 33548 (a new species of thecelsaurid), and $99.214 \pm 0.079/-0.051$ Ma for NCSM 25022 (a new species of ceratopsian). In-field observations of sample sites WS10 (Cifelli Quarry 2) and WS19 initially indicated patterns of post-emplacement alteration or hydraulic reworking (Fig. 1) (Cifelli et al., 1997, 1999). This prediction was corroborated by our zircon dating,

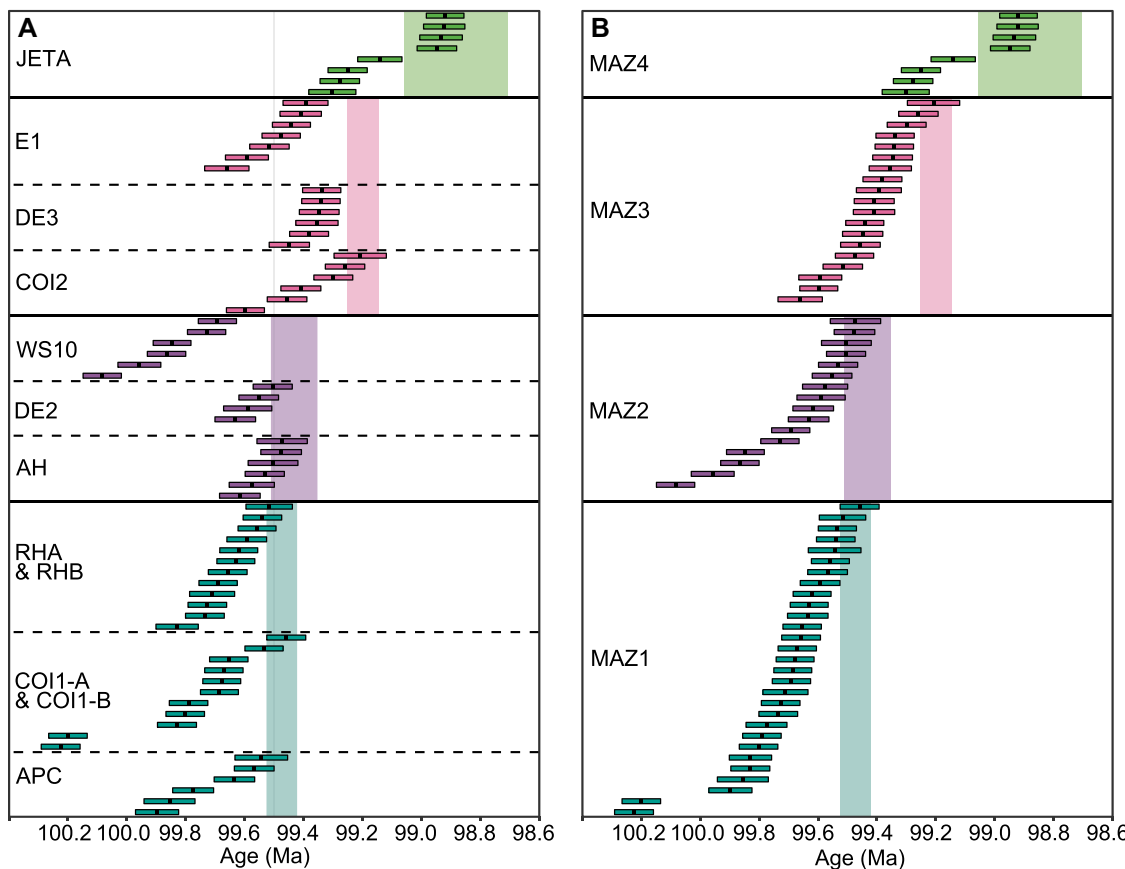


Figure 3. Ranked chemical abrasion-isotope dilution-thermal ionization mass spectrometry $^{206}\text{Pb}/^{238}\text{U}$ zircon dates from the Mussentuchit Member grouped by individual samples (A) and combined into each of MAZ1–MAZ4 (B). Colored fields illustrate depositional ages (2σ uncertainties [error bars]) for ash beds derived by using all U-Pb zircon dates in each ash zone and the Bayesian algorithm of Keller et al. (2018), used as age likelihoods in the model.

with WS19 lacking any young zircon and WS10 containing epiclastic grains that are older than the eruption and parautochthonous fossil fragments. We confirm that the youngest LA-ICP-MS dates provided by Tucker et al. (2020) were biased by Pb loss and thus do not represent the depositional age.

We observed disparities in vertebrate fossil abundance patterns within the Mussentuchit Member. Specifically, most fossils are preserved in tight association with MAZ1–MAZ2 and the middle sandstone (Fig. 4), including two localities (an associated hadrosaur and a disassociated theropod and microvertebrate fossil bonebed) that are entombed directly within MAZ2. Other key vertebrate fossil sites are clustered around MAZ3 in the upper Mussentuchit Member. In contrast, zones of the lower- and uppermost Mussentuchit Member lacking bedded ashes are relatively depauperate of well-preserved macrovertebrate fossils (Fig. 4).

Multiple non-mutually-exclusive factors could produce this apparent preservation pattern. First, despite extensive surveys of the Mussentuchit Member in recent decades, collection bias exists in the paleontological data. Researchers are more likely to document and excavate fossil localities containing associated individuals, new taxa, or abundant remains (bonebeds). Although our distribution data may not capture isolated to poorly preserved materials, this bias does not negate the observed trend of macrovertebrate

site clustering, which minimally represents disparities in preservation mode. The pattern may also be linked to variable depositional conditions observed between the lower and upper Mussentuchit Member (Tucker et al., 2022), mainly related to the emplacement of the middle sandstone; yet this does not explain the pattern observed proximal to MAZ3.

Alternatively, the increase in preservation potential may be linked directly to the ashes themselves. Ramezani et al. (2022) discussed a tight association between fossil richness and volcanic activity in younger, Campanian-age strata across the Western Interior Basin and suggested changes in climate and habitability (Lu et al., 2021) or increases in preservation potential linked to the diagenesis of volcanic sediments as potential drivers. Our findings extend the relationship between fossil abundance and volcanic sedimentation across >20 m.y. of the tectonic evolution of the Western Interior Basin. Thus, the landward paralic setting of the Mussentuchit Member would have simultaneously been a collection point for volcaniclastic ash and other volcano-sedimentary detritus along with a distributary system to the outboard distal shelf and slope depocenters (Lee et al., 2018; Tucker et al., 2022). Thus, the Mussentuchit Member may have played a role in the fertilization of nutrients into the Western Interior Sea of North America, perhaps resulting in a carbon sink that is reflected in the global cool-

ing trend between Ocean Anoxic Event 1d and an antecedent trigger for Ocean Anoxic Event 2 (Wang et al., 2014; Barral et al., 2017; Lee et al., 2018). Our high-resolution temporal framework of the Mussentuchit Member provides unprecedented refinement for addressing questions of biotic responses to tectonism, landscape modification, and climate change just before the Cretaceous Thermal Maximum. As a result, we can provide significantly improved temporal insights into the Albian–Cenomanian transition during a climatic recovery phase just after Ocean Anoxic Event 1d in Utah and across western North America.

ACKNOWLEDGMENTS

We thank members of the 2012–2022 North Carolina Museum of Natural Sciences and Field Museum of Natural History–University of Minnesota expeditions along with R. Cifelli and S. Madsen for relocating historical sites and staff of the Price Field Office, Bureau of Land Management, Utah State Office, and Utah Geological Survey for permitting. Financial support was provided by Stellenbosch University’s Department of Earth Sciences, Canyonlands Natural History Association, and National Science Foundation awards 1925973 and 1925884. We also thank S. Verry and XRA Analytical and Consulting and L. Herzog for logistic support. Any opinions, findings, conclusions, or recommendations expressed in this material are those of the authors and do not necessarily reflect the views of the National Science Foundation. Furthermore, we thank senior editor W. Clyde along with reviewers E.M. Roberts, A. Möller, and anonymous reviewers who significantly improved this manuscript’s earlier versions.

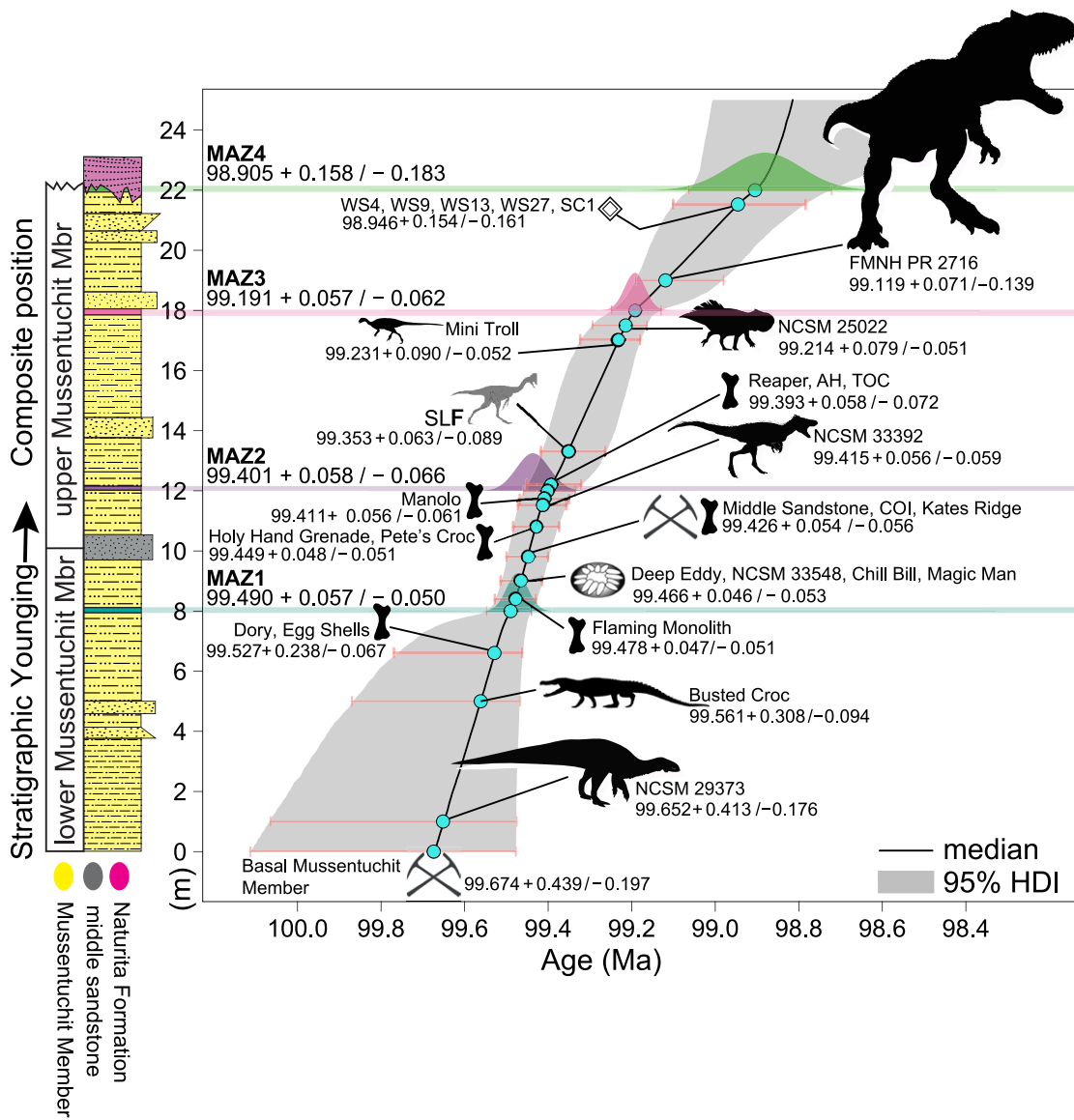


Figure 4. Bayesian age-stratigraphic model for the Mussentuchit Member constructed using our composite stratigraphy and depositional ages for Mussentuchit ash zones MAZ1–MAZ4 (Figs. 2 and 3) and the modified Bchron Bayesian age-stratigraphic model (Trayler et al., 2020). See Figure 2A for sample locations. Posterior ages and uncertainties for stratigraphic positions are interpreted from the median and 95% highest-density intervals (HDI) of the model runs. Model runs were truncated above using a 95.6 Ma age for the overlying Naturita Formation (Tucker et al., 2020). Taxon silhouettes by J. Gonzalez, Z. Lukas, M. Doughty, and phylopic.org under license Public Domain Dedication 1.0.

REFERENCES CITED

Barral, A., Gomez, B., Fourel, F., Daviero-Gomez, V., and Lécuyer, C., 2017, CO₂ and temperature decoupling at the million-year scale during the Cretaceous Greenhouse: *Scientific Reports*, v. 7, 8310, <https://doi.org/10.1038/s41598-017-08234-0>.

Beveridge, T.L., Roberts, E.M., Ramezani, J., Titus, A.L., Eaton, J.G., Irmis, R.B., and Sertich, J.J.W., 2022, Refined geochronology and revised stratigraphic nomenclature of the Upper Cretaceous Wahweap Formation, Utah, U.S.A. and the age of early Campanian vertebrates from southern Laramidia: *Palaeogeography, Palaeoclimatology, Palaeoecology*, v. 591, <https://doi.org/10.1016/j.palaeo.2022.110876>.

Cifelli, R.L., Kirkland, J.I., Weil, A., Deino, A.L., and Kowallis, B.J., 1997, High-precision ⁴⁰Ar/³⁹Ar geochronology and the advent of North America's Late Cretaceous terrestrial fauna: *Proceedings of the National Academy of Sciences of the United States of America*, v. 94, p. 11,163–11,167, <https://doi.org/10.1073/pnas.94.21.11163>.

Cifelli, R.L., Nydam, R.L., Gardner, J.D., Weil, A., Eaton, J.G., Kirkland, J.I., and Madsen, S.K., 1999, Medial Cretaceous vertebrates from the Cedar Mountain Formation, Emery County, Utah: The Mussentuchit local fauna, in Gillette, D.D., ed., *Vertebrate Paleontology in Utah: Utah Geological Survey Miscellaneous Publication 99-1*, p. 219–242.

Eberth, D.A., and Kamo, S.L., 2020, High-precision U-Pb CA-ID-TIMS dating and chronostratigraphy of the dinosaur-rich Horseshoe Canyon Formation (Upper Cretaceous, Campanian–Maastrichtian), Red Deer River Valley, Alberta, Canada: *Canadian Journal of Earth Sciences*, v. 57, p. 1220–1237, <https://doi.org/10.1139/cjes-2019-0019>.

Garrison, J.R., Jr., Brinkman, D., Nichols, D.J., Layer, P., Burge, D., and Thayn, D., 2007, A multidisciplinary study of the Lower Cretaceous Cedar Mountain Formation, Mussentuchit Wash, Utah: A determination of the paleoenvironment and paleoecology of the *Eolambia caroljonesa* dinosaur quarry: *Cretaceous Research*, v. 28, p. 461–494, <https://doi.org/10.1016/j.cretres.2006.07.007>.

Hain, M.P., Sigman, D.M., and Haug, G.H., 2014, The biological pump in the past, in Mottl, M.J., and Elderfield, H., eds., *Treatise on Geochemistry* (2nd edition), Volume 8: The Oceans and Marine Geochemistry, p. 485–517, <https://doi.org/10.1016/B978-0-08-095975-7.00618-5>.

Hintze, L.F., Willis, G.C., Laes, D.Y.M., Sprinkel, D.A., and Brown, K.D., 2000, Digital geologic map of Utah: Utah Geological Survey Map 179DM, scale 1:500,000, <https://doi.org/10.34191/M-179dm>.

Huff, W.D., 2016, K-bentonites: A review: *American Mineralogist*, v. 101, p. 43–70, <https://doi.org/10.2138/am-2016-5339>.

Huybers, P., 2007, Glacial variability over the last two million years: An extended depth-derived age model, continuous obliquity pacing, and the Pleistocene progression: *Quaternary Science Reviews*, v. 26, p. 37–55, <https://doi.org/10.1016/j.quascirev.2006.07.013>.

Huybers, P., 2011, Combined obliquity and precession pacing of late Pleistocene deglaciations: *Nature*, v. 480, p. 229–232, <https://doi.org/10.1038/nature10626>.

Keller, C.B., Schoene, B., and Samperton, K.M., 2018, A stochastic sampling approach to zircon eruption age interpretation: *Geochemical Perspectives Letters*, v. 8, p. 31–35, <https://doi.org/10.7185/geochemlet.1826>.

Kirkland, J.I., Suarez, M., Suarez, C., and Hunt-Foster, R., 2016, The Lower Cretaceous in east-central Utah—The Cedar Mountain Formation and its

bounding strata: Geology of the Intermountain West, v. 3, p. 101–228, <https://doi.org/10.31711/giw.v3.pp101-228>.

Laskowski, A.K., DeCelles, P.G., and Gehrels, G.E., 2013, Detrital zircon geochronology of Cordilleran retroarc foreland basin strata, western North America: *Tectonics*, v. 32, p. 1027–1048, <https://doi.org/10.1002/tect.20065>.

Lee, C.-T.A., Jiang, H.H., Ronay, E., Minisini, D., Stiles, J., and Neal, M., 2018, Volcanic ash as a driver of enhanced organic carbon burial in the Cretaceous: *Scientific Reports*, v. 8, 4197, <https://doi.org/10.1038/s41598-018-22576-3>.

Lu, J., Zhang, P.X., Dal Corso, J., Yang, M.F., Wiggnall, P.B., Greene, S.E., Shao, L.Y., Lyu, D., and Hilton, J., 2021, Volcanically driven lacustrine ecosystem changes during the Carnian Pluvial Episode (Late Triassic): *Proceedings of the National Academy of Sciences of the United States of America*, v. 118, <https://doi.org/10.1073/pnas.2109895118>.

Mattinson, J.M., 2005, Zircon U-Pb chemical abrasion (“CA-TIMS”) method: Combined annealing and multi-step partial dissolution analysis for improved precision and accuracy of zircon ages: *Chemical Geology*, v. 220, p. 47–66, <https://doi.org/10.1016/j.chemgeo.2005.03.011>.

Miall, A., ed., 2008, *Sedimentary Basins of the United States and Canada*: Amsterdam, Elsevier Science & Technology, *Sedimentary Basins of the World*, v. 5, 624 p.

Ramezani, J., Beveridge, T.L., Rogers, R.R., Eberth, D.A., and Roberts, E.M., 2022, Calibrating the zenith of dinosaur diversity in the Campanian of the Western Interior Basin by CA-ID-TIMS U-Pb geochronology: *Scientific Reports*, v. 12, 16026, <https://doi.org/10.1038/s41598-022-19896-w>.

R Core Team, 2020, R: A language and environment for statistical computing: Vienna, Austria, R Foundation for Statistical Computing, <https://www.R-project.org/>.

Rossignol, C., et al., 2019, Using volcaniclastic rocks to constrain sedimentation ages: To what extent are volcanism and sedimentation synchronous?: *Sedimentary Geology*, v. 381, p. 46–64, <https://doi.org/10.1016/j.sedgeo.2018.12.010>.

Schoene, B., Eddy, M.P., Samperton, K.M., Keller, C.B., Keller, G., Adatte, T., and Khadri, S.F., 2019, U-Pb constraints on pulsed eruption of the Deccan Traps across the end-Cretaceous mass extinction: *Science*, v. 363, p. 862–866, <https://doi.org/10.1126/science.aau2422>.

Schoene, B., Eddy, M.P., Keller, C.B., and Samperton, K.M., 2021, An evaluation of Deccan Traps eruption rates using geochronologic data: *Geochronology*, v. 3, p. 181–198, <https://doi.org/10.5194/gchron-3-181-2021>.

Schwartz, T.M., Surpless, K.D., Colgan, J.P., Johnstone, S.A., and Holm-Denoma, C.S., 2021, Detrital zircon record of magmatism and sediment dispersal across the North American Cordilleran arc system (28–48°N): *Earth-Science Reviews*, v. 220, <https://doi.org/10.1016/j.earscirev.2021.103734>.

Sharman, G.R., and Malkowski, M.A., 2020, Needles in a haystack: Detrital zircon U-Pb ages and the maximum depositional age of modern global sediment: *Earth-Science Reviews*, v. 203, <https://doi.org/10.1016/j.earscirev.2020.103109>.

Singer, B.S., Jicha, B.R., Sawyer, D., Walaszczyk, I., Buchwaldt, R., and Mutterlose, J., 2021, Geochronology of late Albian–Cenomanian strata in the U.S. Western Interior: *Geological Society of America Bulletin*, v. 133, p. 1665–1678, <https://doi.org/10.1130/B35794.1>.

Trayler, R.B., Schmitz, M.D., Cuitiño, J.I., Kohn, M.J., Bargo, M.S., Kay, R.F., Strömborg, C.A.E., and Vizcaíno, S.F., 2020, An improved approach to age-modeling in deep time: Implications for the Santa Cruz Formation, Argentina: *Geological Society of America Bulletin*, v. 132, p. 233–244, <https://doi.org/10.1130/B35203.1>.

Tucker, R.T., Zanno, L.E., Huang, H.Q., and Makovicky, P.J., 2020, A refined temporal framework for newly discovered fossil assemblages of the upper Cedar Mountain Formation (Mussentuchit Member), Mussentuchit Wash, Central Utah: *Cretaceous Research*, v. 110, <https://doi.org/10.1016/j.cretres.2020.104384>.

Tucker, R.T., Suarez, C.A., Makovicky, P.J., and Zanno, L.E., 2022, Paralic sedimentology of the Mussentuchit Member coastal plain, Cedar Mountain Formation, central Utah, U.S.A.: *Journal of Sedimentary Research*, v. 92, p. 546–569, <https://doi.org/10.2110/jsr.2021.028>.

Vermeesch, P., 2021, Maximum depositional age estimation revisited: *Geoscience Frontiers*, v. 12, p. 843–850, <https://doi.org/10.1016/j.gsf.2020.08.008>.

Wang, Y.D., Huang, C.M., Sun, B.N., Quan, C., Wu, J.Y., and Lin, Z.C., 2014, Paleo-CO₂ variation trends and the Cretaceous greenhouse climate: *Earth-Science Reviews*, v. 129, p. 136–147, <https://doi.org/10.1016/j.earscirev.2013.11.001>.

Wotzlaw, J.-F., Bindeman, I.N., Watts, K.E., Schmitt, A.K., Caricchi, L., and Schaltegger, U., 2014, Linking rapid magma reservoir assembly and eruption trigger mechanisms at evolved Yellowstone-type supervolcanoes: *Geology*, v. 42, p. 807–810, <https://doi.org/10.1130/G35979.1>.

Printed in the USA